



Synthesis and preliminary evaluation of a novel positron emission tomography (PET) ligand for imaging fatty acid amide hydrolase (FAAH)



Zhen Chen^{b,1}, Lu Hou^{a,1}, Jiefeng Gan^a, Qijun Cai^a, Weijian Ye^a, Jiahui Chen^{a,b}, Zhiqiang Tan^a, Chao Zheng^c, Guocong Li^a, Hao Xu^a, Christopher J. Fowler^d, Steven H. Liang^{b,*}, Lu Wang^{a,*}

^a Center of Cyclotron and PET Radiopharmaceuticals, Department of Nuclear Medicine and PET/CT-MRI Center, The First Affiliated Hospital of Jinan University, Guangzhou 510630, China

^b Division of Nuclear Medicine and Molecular Imaging, Massachusetts General Hospital & Department of Radiology, Harvard Medical School, Boston, MA 02114, USA

^c Athinoula A. Martinos Center for Biomedical Imaging, Massachusetts General Hospital & Department of Radiology, Harvard Medical School, Charlestown, Boston, MA 02129, USA

^d Department of Integrative Medical Biology, Umeå University, SE-901 87 Umeå, Sweden

ARTICLE INFO

Keywords:

Fatty acid amide hydrolase
FAAH
PET
[¹¹C]FAAH-1906
Reversible binding

ABSTRACT

Fatty acid amide hydrolase (FAAH) exerts its main function in the catabolism of the endogenous chemical messenger anandamide (AEA), thus modulating the endocannabinoid (eCB) pathway. Inhibition of FAAH may serve as an effective strategy to relieve anxiety and possibly other central nervous system (CNS)-related disorders. Positron emission tomography (PET) would facilitate us to better understand the relationship between FAAH in certain disease conditions, and accelerate clinical translation of FAAH inhibitors by providing *in vivo* quantitative information. So far, most PET tracers show irreversible binding patterns with FAAH, which would result in complicated quantitative processes. Herein, we have identified a new FAAH inhibitor (1-((1-methyl-1H-indol-2-yl)methyl)piperidin-4-yl)(oxazol-2-yl)methanone (**8**) which inhibits the hydrolysis of AEA in the brain with high potency (IC₅₀ value 11 nM at a substrate concentration of 0.5 μM), and without showing time-dependency. The PET tracer [¹¹C]**8** (also called [¹¹C]FAAH-1906) was successfully radiolabeled with [¹¹C]MeI in 17 ± 6% decay-corrected radiochemical yield (*n* = 7) with > 74.0 GBq/μmol (2 Ci/μmol) molar activity and > 99% radiochemical purity. *Ex vivo* biodistribution and blocking studies of [¹¹C]**8** in normal mice were also conducted, indicating good brain penetration, high brain target selectivity, and modest to excellent target selectivity in peripheral tissues. Thus, [¹¹C]**8** is a potentially useful PET ligand with enzyme inhibitory and target binding properties consistent with a reversible mode of action.

The endocannabinoid (eCB) system is fundamental to physiology, and has widespread influences on the central nervous system (CNS), immune system and other organs.¹ Abnormalities of eCB system have been implicated in many pathological processes such as inflammation, pain, cognition, neuropsychiatric and metabolic disorders.^{2,3} Δ⁹-tetrahydrocannabinol (Δ⁹-THC), as the principal psychoactive component of cannabis and hashish,⁴ has been known to have potentially useful medicinal in addition to its narcotic effects on the eCB system by mediating the cannabinoid receptors CB₁ and CB₂.¹ In addition, anandamide (AEA)⁵ and 2-arachidonic acid glycerol (2-AG),^{6,7} which are synthesized “on demand” following Ca²⁺ increasing in the postsynaptic cell, serve as the endogenous chemical messengers to activate CB₁ and CB₂ receptors. These two endocannabinoids undergo *in vivo* degradation by enzymatic hydrolysis and by oxidation.⁸ In the brain, fatty acid

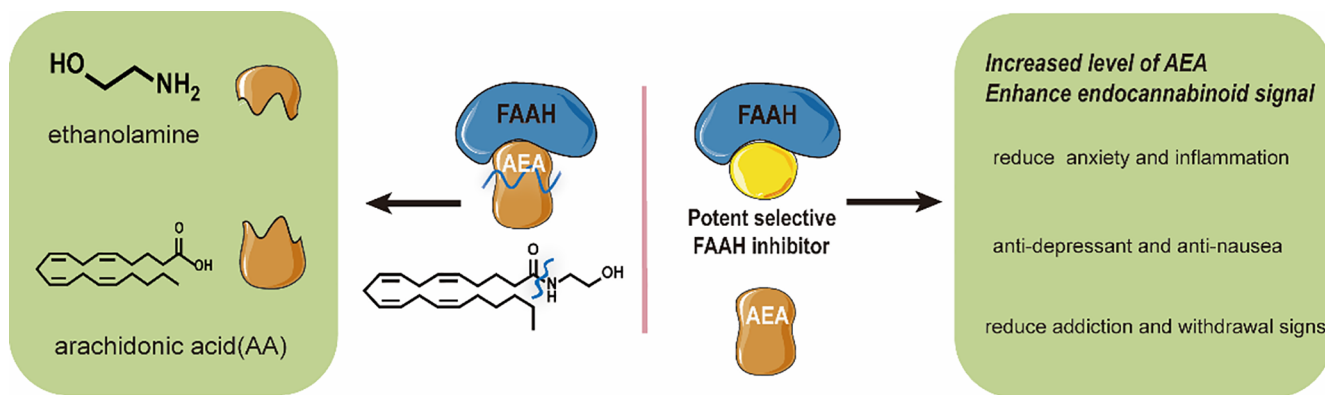
amide hydrolase (FAAH) is the principal hydrolytic enzyme for AEA, whilst monoacylglycerol lipase (MAGL) is primarily responsible for 2-AG catabolism.^{9,10}

FAAH is an intact mammalian membrane enzyme which involves an unusual serine-serine-lysine (Ser241-Ser217-Lys142) catalytic triad, and categorized as a serine hydrolase.¹¹ The immunohistochemical analysis of the hippocampal and olfactory brain cortex in patients with Alzheimer's disease (AD) revealed that FAAH was selectively over-expressed in the astrocytes and microglia related to neural plaques, and its hydrolytic activity was significantly up-regulated in plaques and surrounding areas.¹² Besides, in terms of Huntington's disease (HD), FAAH activity was found to be decreased to a certain extent in the central nervous system of patients compared with normal.¹³ In pre-clinical studies, inhibition of FAAH resulted in elevated levels of AEA,¹⁴

* Corresponding authors.

E-mail addresses: liang.steven@mgh.harvard.edu (S.H. Liang), l_wang1009@jnu.edu.cn (L. Wang).

¹ These two authors contributed equally to this work.



Scheme 1. Mechanism of FAAH for modulating eCB system and therapeutic potential for FAAH Inhibitors.

which interacted with cannabinoid receptors to induce anti-inflammatory, analgesic, antidepressant and anxiolytic properties in animal models^{15–17} without producing the sort of behavioral effects seen with directly acting CB₁ receptor agonists (Scheme 1).^{18,19} The above observations suggest FAAH may be a useful and valuable therapeutic target in the central nervous system that may exert critical impacts on neuro-disorders. Therefore, recent research efforts have been shifted to the development of FAAH inhibitors, including URB597,¹⁸ PF-04457845,^{20–23} JNJ-42165279,²⁴ V158866²⁵ and SSR411298,²⁶ some of which have been advanced to clinical trials for treating anxiety, osteoarthritis pain, cannabis withdrawal and schizophrenia. In general, these compounds are well-tolerated with one exception that compound BIA 10–2474 exhibited severe adverse effects most likely due to off-target actions.^{27,28}

Positron emission tomography (PET) is a noninvasive imaging technology with high sensitivity and specificity. Based on a specific ligand bearing a positron-emitting radionuclide (“PET tracer”), PET can quantify biological information on the molecular level, which is feasible for PET to assist disease diagnosis, treatment evaluation, and drug development.^{29–31} Unlike fluorescence imaging,³² PET technique has greater tissue penetration, and, the radiotracer used for imaging is microdose (10^{-6} – 10^{-9} g), which makes it possible to assess biological processes without pharmacological effects, thereby accelerating the clinical translation and transformation for candidate drugs.³³ PET imaging studies of FAAH would allow better understanding of distribution, expression and functions of this enzyme under physiological and pathological conditions. Developing FAAH targeted PET tracers would not only be helpful for early diagnosis of clinical neurological diseases such as depression, AD and HD, but also facilitate the clinical translation of FAAH-related drugs by providing insight into *in vivo* pharmacokinetics, target occupancy and dose selection. As shown in Fig. 1, in recent years, continued efforts have been concentrated on the development of suitable PET tracers for imaging FAAH, including [¹¹C]CURB ([¹¹C]1),³⁴ [¹¹C]URB597 ([¹¹C]2) and analogues,³⁵ [¹⁸F]DOPP ([¹⁸F]3),^{36,37} [¹¹C]PF-04457845 ([¹¹C]4),³⁸ and [¹⁸F]PF-9811 ([¹⁸F]5),³⁹ all of which share the common feature of covalent and irreversible binding.^{40,41} Among them, [¹¹C]1 has been studied for FAAH imaging in patients with several neurological diseases. The level of FAAH in adult and young cannabis users decreased significantly.^{42,43} Brain imaging in psychiatric patients showed that FAAH activity was negatively correlated with positive psychotic symptom severity.⁴⁴ In terms of borderline personality disorder patients, the FAAH activity in amygdala-prefrontal cortex measured by [¹¹C]1 PET signals was elevated by 11% and positively correlated with hostility/anger.⁴⁵

In contrast to irreversible FAAH PET tracers, the development of reversible FAAH PET tracers is still in its infancy. To date, only two reversible PET ligands for FAAH imaging, namely [¹¹C]MK-3168 ([¹¹C]

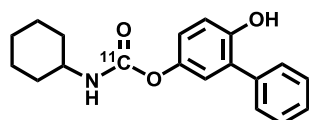
6) and [¹¹C]MPPO ([¹¹C]7), have been reported by Merck researchers⁴⁶ and our groups⁴⁷, respectively. Despite that [¹¹C]6 has been advanced to preliminary human PET studies since 2012, only limited results were disclosed in the form of conference proceedings.^{24,48,49} Compound [¹¹C]7 was developed based on a novel α -keto(pyridinyl)oxazolyl structures, although it demonstrated an excellent *in vitro* FAAH inhibitory potency (IC₅₀ 10 nM),⁵⁰ unsatisfactory brain penetration and marginal *in vivo* specificity prevents its further evaluation.⁴⁷ Therefore, it is an unmet need for the development of new reversible FAAH PET tracers with improved blood-brain-barrier (BBB) penetration ability and *in vivo* specificity.

As our continuous interest in the development of reversible FAAH PET tracers based on α -keto-heterocyclic scaffold, which has already demonstrated suitable enzyme inhibitory potency as well as a clear reversible binding mechanism,⁵¹ herein we aimed to discover a new α -keto-heterocyclic skeleton with improved BBB penetration ability and *in vivo* specificity. Janssen Pharmaceutica revealed that α -keto-oxazolyl structures exhibited good to excellent binding affinities to FAAH,^{52,53} which could serve as promising candidates of PET tracers. Considering the feasibility of radiolabeling as well as the successful and effective contributions of indole moieties in drug development,^{54,55} we selected (1-((1-methyl-1*H*-indol-2-yl)methyl)piperidin-4-yl)(oxazol-2-yl)methanone (**8**) for radiolabeling and further exploration. Herein, we describe our chemical synthesis, pharmacological and physicochemical evaluation, radiosynthesis and preliminary evaluation of (1-((1-¹¹C-methyl-1*H*-indol-2-yl)methyl)piperidin-4-yl)(oxazol-2-yl)methanone ([¹¹C]FAAH-1906, [¹¹C]**8** in Fig. 1) *in vivo* by PET.

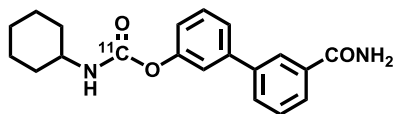
With FAAH inhibitor **8** as the molecule of interest, we conducted an efficient four-step synthesis. As summarized in Scheme 2, condensation of carboxylic acid **9** with *N*-methoxymethylamine hydrochloride in the presence of HUBT under basic conditions afforded the Weinreb amide **10** in 93% yield. As optimized in our previous work,⁴⁷ the following nucleophilic substitution was successfully realized by *i*PrMgCl in THF, leading to key intermediate oxazolyl piperidine **11** in 49% yield. Deprotection of compound **11** in acidic conditions gave ammonium salt **12**, which was used without further purification to undergo a reductive amination with indole-2-carboxaldehyde to generate the labeling precursor **13** in 39% yield. In terms of standard compound **8**, a similar reductive amination was performed with 1-methylindole-2-carboxaldehyde, and the FAAH inhibitor **8** was obtained in 43% yield.

We determined the inhibitory potency of **8** *in vitro* towards the FAAH-catalysed hydrolysis of 0.5 μ M [³H]-anandamide ([³H]AEA) in rat brain homogenates. In the assay employed here, the irreversible FAAH inhibitor DOPP (**3**) inhibits in nM concentrations [³H]AEA hydrolysis in a manner dependent upon the preincubation time (as expected for an irreversible inhibitor) used [33]. As shown in Fig. 2, compound **8** concentration-dependently inhibits rat brain [³H]AEA

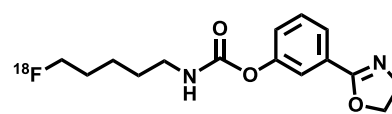
Irreversible



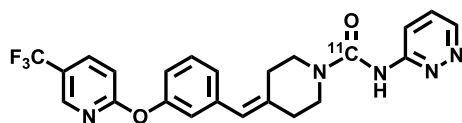
[¹¹C]CURB ([¹¹C]1)
2011



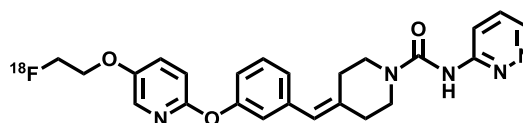
[¹¹C]URB597 ([¹¹C]2)
2010



[¹⁸F]DOPP ([¹⁸F]3)
2013

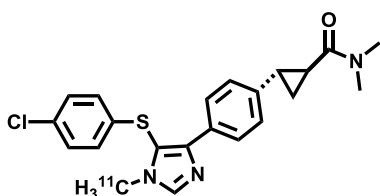


[¹¹C]PF-04457845 ([¹¹C]4)
2013

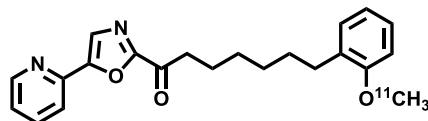


[¹⁸F]PF-9811 ([¹⁸F]5)
2012

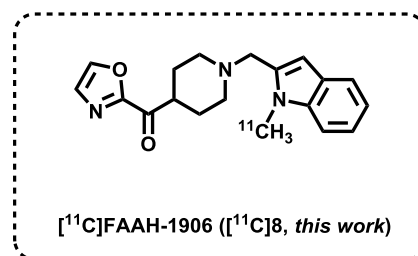
Reversible



[¹¹C]MK-3168 ([¹¹C]6)
2013



[¹¹C]MPP0 ([¹¹C]7)
2015



[¹¹C]FAAH-1906 ([¹¹C]8, this work)

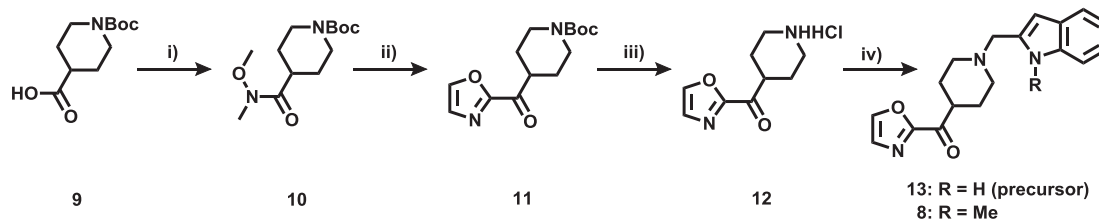
Fig. 1. Representative PET tracers for imaging FAAH.

hydrolysis with an IC_{50} value of 13.3 ± 3.7 nM. In addition, no obvious increase of the inhibitory potency of **8** was detected following a 60 min preincubation phase between enzyme and inhibitor ($IC_{50} = 11.5 \pm 2.3$ nM). The physicochemical properties are essential factors for the prediction of BBB permeability. Therefore, calculated partition coefficient (CLogP), calculated distribution coefficient at pH = 7.4 (CLogD), molecular weight (MW), topological polar surface (TPSA), number of hydrogen bond donors (HBD), and ionization constant of the most basic center (pK_a) of compound **8** were predicted by ACD/Labs software (2019.2.1 version). As shown in Table 1, all the values lie in the favorable range for a brain imaging PET tracer, with CNS PET multiparameter optimization (MPO) scores as 5.2.⁵⁶

The favorable pharmacological and physicochemical properties prompted us to radiolabel and further evaluate compound **8**. As shown in Scheme 3, the nitrogen atom on the indole ring in **13** was considered as the most efficient labeling site for **8** with [¹¹C]CH₃I.⁵⁷ A module of GE TRACERlab FX MeI was adopted for the automated synthesis of [¹¹C]**8**, which included radiolabeling, HPLC purification and

formulation. The radiosynthesis of [¹¹C]**8** was carried out by heating a mixture of the indole precursor **13**, [¹¹C]CH₃I, KOH and dimethylsulfoxide (DMSO) to 130 °C for 5 min. The reaction mixture was then diluted and purified by a semi-preparative reverse high-performance liquid chromatography (HPLC) to give [¹¹C]**8**, which was then formulated in saline containing 10% ethanol. As a result, [¹¹C]**8** was isolated in $17 \pm 6\%$ ($n = 7$) radiochemical yield (RCY, decay-corrected) relative to starting [¹¹C]CO₂ at the end of synthesis (EOS) with excellent radiochemical purity (> 99%), and high molar activity (> 74.0 GBq/μmol (2.0 Ci/μmol)). In addition, no radiolysis was detected up to 90 min after formulation, indicating the radiochemical stability was sufficient for subsequent studies.

The LogD of [¹¹C]**8** was determined by the Shake Flask method⁵⁸ as 2.90 ± 0.01 , falling within the optimal range for a neurological PET tracer.⁴⁰ This value is comparable with [¹¹C]CURB ([¹¹C]1, LogD 2.8),³⁴ and lower than our previous reported reversible PET tracer [¹¹C]MPP0 ([¹¹C]7, LogD 3.43),⁴⁷ which may improve brain penetration and decrease non-specific binding *in vivo*.



Scheme 2. Chemical synthesis of precursor (**13**) and standard (**8**) for [¹¹C]**8** radiolabeling. Reagents and conditions: (i) *N*-methoxymethylamine hydrochloride, HBTU, DIPEA, DMF, 93%; (ii) oxazole, iPrMgCl, THF, -15 °C, 49%; (iii) HCl, dioxane, 70 °C, 91%; (iv) indole-2-carboxaldehyde or 1-methylindole-2-carboxaldehyde, NaBH(OAc)₃, TEA, DCE, 39% for **13**; 43% for **8**.

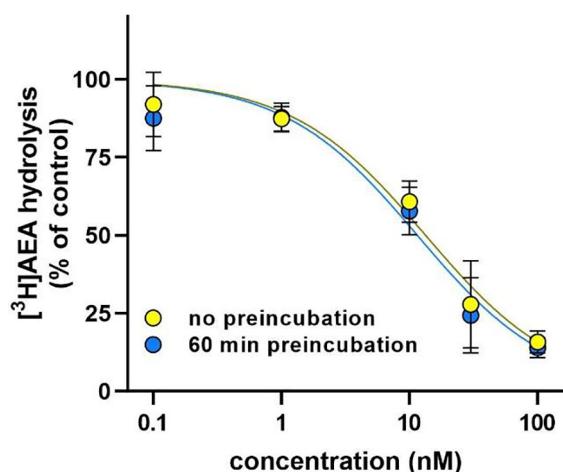


Fig. 2. Inhibition by **8** of the hydrolysis of 0.5 μM [^3H]AEA in rat brain homogenates. Shown are means \pm s.e.m., $n = 3$ (except for the data at 30 μM inhibitor, where the mean and range for two experiments is shown), of the activity as % of vehicle control following either no preincubation (blue symbols) or 60 min preincubation (yellow symbols) between the enzyme source and **8** prior to addition of substrate.

Table 1
Physicochemical properties prediction of **8**.^a

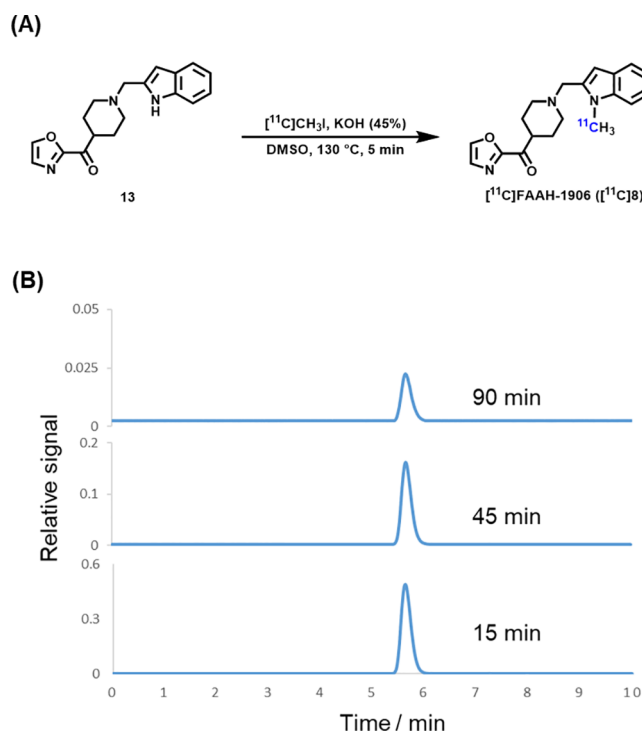
CLogP	2.13	TPSA	51.27
CLogD	1.87	HBD	0
MW	323.39	pKa	7.6

			
<div style="border: 1px dashed black; padding: 5px; display: inline-block;"> MPO 5.2 </div>			

^a Data were calculated by ACD/Labs software (2019.2.1 version).

Pharmacokinetic properties, the uptake, distribution and clearance of [^{11}C]**8** were studied in mice at four time points (5, 15, 30 and 60 min) after tracer injection. The experimental results were described as the percentage of injected dose per gram of wet tissue (%ID/g) in Fig. 3. The radioactivity of [^{11}C]**8** was washed out efficiently from blood with the ratio of %ID/ $g_{5\text{min}/60\text{min}}$ as 2, and the similar results was also observed in [^{11}C]**7** (ratio of %ID/ $g_{5\text{min}/60\text{min}}$ as 2.3).⁴⁷ High radioactivity levels (> 5 %ID/g) were observed in several organs including spleen, heart, lungs, pancreas, small intestine, kidneys and liver within the initial 5 min. After that, the signals in most organs decreased rapidly, while the radioactivity in the stomach and liver continually increased until 15 min and then washed out gradually, and the radioactive signal in the small intestine reached the plateau at 30 min. These results, together with high radioactivity levels in the small intestine, kidneys, and liver at 60 min post tracer injection, possibly indicated a combined urinary and hepatobiliary elimination pathway.

Notably, high brain uptake (ca. 9.2 %ID/g) was detected after 5 min post tracer injection, then followed by a rapid washout (ratios of %ID/ $g_{5\text{min}/30\text{min}}$ and %ID/ $g_{5\text{min}/60\text{min}}$ as 4.7 and 12.7, respectively), which, together with the lack of time-dependency of **8** towards [^3H]AEA hydrolysis shown in Fig. 1 are consistent with a reversible binding pattern. To verify *in vivo* specific binding, mice ($n = 4$) in two time points (5 and 30 min) were pretreated with URB597 (3 mg/kg, *i.v.*) 30 min prior to [^{11}C]**8** injection. The brain uptake was significantly decreased by ~35% with pretreatment of URB597 (3 mg/kg, *i.v.*) at two time points



Scheme 3. Radiosynthesis of [^{11}C]**8** (A) and *in vitro* stability test (B).

(5 and 30 min) (Fig. 4), indicating that [^{11}C]**8** showed good *in vivo* target selectivity in the mouse brain. Radioactivity was also significantly decreased in the lungs, pancreas and kidneys ($p < 0.05$), demonstrating modest to excellent target selectivity in peripheral tissues (Figs. S1 and S2 in Supporting Information).

In conclusion, we have prepared an improved heterocyclic FAAH inhibitor **8**, in which the indole moiety was amenable for ^{11}C radiolabeling. The preliminary pharmacological and physicochemical evaluations were conducted, and the corresponding PET tracer [^{11}C]FAAH-1906 ([^{11}C]**8**) was automatically produced in excellent radiochemical yields and high molar activities. The *ex vivo* biodistribution studies (and [^3H]AEA hydrolysis studies) are consistent with a reversible interaction between **8** and FAAH. Further, [^{11}C]**8** exhibited high brain permeability and moderate specific binding. In order to obtain in-depth pharmacokinetic information and regional distribution of [^{11}C]**8** in the brain, further PET imaging study in rodents and/or non-human primates, together with kinetic modeling is necessary to provide pharmacological information and access the potential of [^{11}C]**8** for clinical translation.

Author contributions

L.W. and S.H.L. conceived and supervised the full project, analyzed the data with Z.C. and L.H.; Z.C. synthesized the compounds with W.Y., J.C. and C.Z., also fulfilled the radiolabeling and quality control; L.H. performed the biodistribution studies with J.G., Q.C., Z.T. and G.L.; C.J.F. contributed to the binding potency testing; H.X. provided insightful suggestions for experiments and data analysis. All authors prepared the manuscript and Supporting Information. H.X. and S.H.L. helped polish the manuscript. All authors have read and agreed to the published version of the manuscript.

Declaration of Competing Interest

The authors declare that they have no known competing financial interests or personal relationships that could have appeared to influence the work reported in this paper.

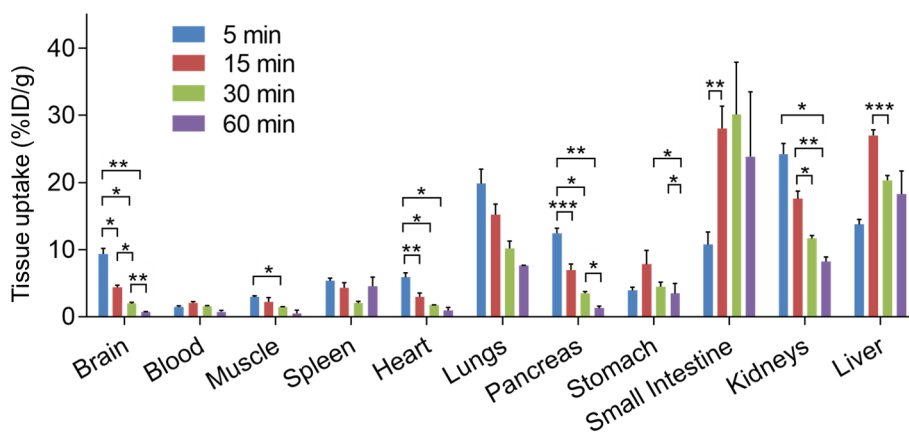


Fig. 3. Whole-body ex vivo biodistribution studies in mice at four different time points (5, 15, 30 and 60 min) post injection of $[^{11}\text{C}]\mathbf{8}$. Data are expressed as %ID/g (mean \pm SD, $n = 4$). %ID/g = injected dose per gram of wet tissue. Asterisks indicate statistical significance. * $p < 0.05$, ** $p \leq 0.01$, and *** $p \leq 0.001$.

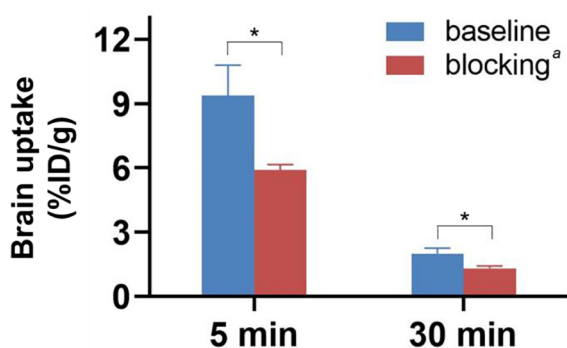


Fig. 4. Brain uptake of $[^{11}\text{C}]\mathbf{8}$ in mice at two time points (5 and 30 min). ^aBlocking conditions: URB597 (3 mg/kg), 30 min i.v. before radioligand injection. Data are expressed as %ID/g (mean \pm SD, $n = 4$). %ID/g = injected dose per gram of wet tissue. Asterisks indicate statistical significance. * $p < 0.05$.

Acknowledgments

The authors acknowledge the National Natural Science Foundation of China (81701751, 81871383), the Fundamental Research Funds for the Central Universities (21619104), and Guangdong Basic and Applied Basic Research Foundation (2020A1515011192). L.W. would like to thank the support of K. C. Wong Education Foundation. C.J.F. would like to thank and the Research Funds of Umeå University Medical Faculty for research support. We would like to thank the staff of the First Affiliated Hospital of Jinan University (JNUH) and Massachusetts General Hospital (MGH) for their support with cyclotron operation and radioisotope production.

Appendix A. Supplementary data

Supplementary data to this article can be found online at <https://doi.org/10.1016/j.bmcl.2020.127513>.

References

- Blankman JL, Cravatt BF. Chemical probes of endocannabinoid metabolism. *Pharmacol Rev*. 2013;65:849–871.
- Ahn K, McKinney MK, Cravatt BF. Enzymatic pathways that regulate endocannabinoid signaling in the nervous system. *Chem Rev*. 2008;108:1687–1707.
- Di Marzo V. Targeting the endocannabinoid system: to enhance or reduce? *Nat Rev Drug Discov*. 2008;7:438–455.
- Gaoni Y, Mechoulam R. Isolation, structure, and partial synthesis of an active constituent of hashish. *J Am Chem Soc*. 1964;86:1646–1647.
- Devane WA, Hanus L, Breuer A, et al. Isolation and structure of a brain constituent that binds to the cannabinoid receptor. *Science (New York, NY)*. 1992;258:1946–1949.
- Mechoulam R, Ben-Shabat S, Hanus L, et al. Identification of an endogenous 2-monoglyceride, present in canine gut, that binds to cannabinoid receptors. *Biochem Pharmacol*. 1995;50:83–90.
- Sugiura T, Kondo S, Suckagawa A, et al. 2-Arachidonoylglycerol: a possible endogenous cannabinoid receptor ligand in brain. *Biochem Biophys Res Commun*. 1995;215:89–97.
- Ueda N, Tsuboi K, Uyama T. Metabolism of endocannabinoids and related N-acyl-ethanolamines: canonical and alternative pathways. *FEBS J*. 2013;280:1874–1894.
- Cravatt BF, Giang DK, Mayfield SP, et al. Molecular characterization of an enzyme that degrades neuromodulatory fatty-acid amides. *Nature*. 1996;384:83–87.
- Dinh TP, Carpenter D, Leslie FM, et al. Brain monoglyceride lipase participating in endocannabinoid inactivation. *Proc Natl Acad Sci USA*. 2002;99:10819–10824.
- McKinney MK, Cravatt BF. Structure and function of fatty acid amide hydrolase. *Annu Rev Biochem*. 2005;74:411–432.
- Benito C, Nunez E, Tolon RM, et al. Cannabinoid CB2 receptors and fatty acid amide hydrolase are selectively overexpressed in neuritic plaque-associated glia in Alzheimer's disease brains. *J Neurosci*. 2003;23:11136–11141.
- Battista N, Bari M, Tarditi A, et al. Severe deficiency of the fatty acid amide hydrolase (FAAH) activity segregates with the Huntington's disease mutation in peripheral lymphocytes. *Neurobiol Dis*. 2007;27:108–116.
- Cravatt BF, Demarest K, Patricelli MP, et al. Supersensitivity to anandamide and enhanced endogenous cannabinoid signaling in mice lacking fatty acid amide hydrolase. *Proc Natl Acad Sci USA*. 2001;98:9371–9376.
- Gaetani S, DiPasquale P, Romano A, et al. The endocannabinoid system as a target for novel anxiolytic and antidepressant drugs. *Int Rev Neurobiol*. 2009;85:57–72.
- Gobbi G, Bambico FR, Mangieri R, et al. Antidepressant-like activity and modulation of brain monoaminergic transmission by blockade of anandamide hydrolysis. *Proc Natl Acad Sci USA*. 2005;102:18620–18625.
- Lichtman AH, Shelton CC, Advani T, et al. Mice lacking fatty acid amide hydrolase exhibit a cannabinoid receptor-mediated phenotypic hypoalgesia. *Pain*. 2004;109:319–327.
- Kathuria S, Gaetani S, Fegley D, et al. Modulation of anxiety through blockade of anandamide hydrolysis. *Nat Med*. 2003;9:76–81.
- Piomelli D. The molecular logic of endocannabinoid signalling. *Nat Rev Neurosci*. 2003;4:873–884.
- Ahn K, Smith SE, Liimatta MB, et al. Mechanistic and pharmacological characterization of PF-04457845: a highly potent and selective fatty acid amide hydrolase inhibitor that reduces inflammatory and noninflammatory pain. *J Pharmacol Exp Ther*. 2011;338:114–124.
- Huggins JP, Smart TS, Langman S, et al. An efficient randomised, placebo-controlled clinical trial with the irreversible fatty acid amide hydrolase-1 inhibitor PF-04457845, which modulates endocannabinoids but fails to induce effective analgesia in patients with pain due to osteoarthritis of the knee. *Pain*. 2012;153:1837–1846.
- Johnson DS, Stiff C, Lazerwith SE, et al. Discovery of PF-04457845: a highly potent, orally bioavailable, and selective urea FAAH inhibitor. *ACS Med Chem Lett*. 2011;2:91–96.
- Li GL, Winter H, Arends R, et al. Assessment of the pharmacology and tolerability of PF-04457845, an irreversible inhibitor of fatty acid amide hydrolase-1, in healthy subjects. *Br J Clin Pharmacol*. 2012;73:706–716.
- Postnov A, Schmidt ME, Pemberton DJ, et al. Fatty Acid amide hydrolase inhibition by JNJ-42165279: a multiple-ascending dose and a positron emission tomography study in healthy volunteers. *Clin Transl Sci*. 2018;11:397–404.
- Pawsey S, Wood M, Browne H, et al. Safety, tolerability and pharmacokinetics of FAAH inhibitor V158866: a double-blind, randomised, placebo-controlled phase I study in healthy volunteers. *Drugs R D*. 2016;16:181–191.
- Griebel G, Stemmelin J, Lopez-Grancha M, et al. The selective reversible FAAH inhibitor, SSR411298, restores the development of maladaptive behaviors to acute and chronic stress in rodents. *Sci Rep*. 2018;8:1–25.
- Gupta Y, Singh H, Sarangi S. French Phase I clinical trial disaster: issues, learning points, and potential safety measures. *J Nat Sc Biol Med*. 2018;9:106.

28. Ni F. Scientists in the dark after fatal French clinical trial. *Nature*. 2016;529:263–264.
29. Phelps ME. Positron emission tomography provides molecular imaging of biological processes. *Proc Natl Acad Sci USA*. 2000;97:9226–9233.
30. Ametamey SM, Honer M, Schubiger PA. Molecular imaging with PET. *Chem Rev*. 2008;108:1501–1516.
31. Willmann JK, van Bruggen N, Dinkelborg LM, et al. Molecular imaging in drug development. *Nat Rev Drug Discov*. 2008;7:591–607.
32. Ma N, Hu J, Zhang ZM, et al. 2H-azirine-based reagents for chemoselective bioconjugation at carboxyl residues inside live cells. *J Am Chem Soc*. 2020;142:6051–6059.
33. Wagner CC, Langer O. Approaches using molecular imaging technology – use of PET in clinical microdose studies. *Adv Drug Deliv Rev*. 2011;63:539–546.
34. Wilson AA, Garcia A, Parkes J, et al. [¹¹C]CURB: evaluation of a novel radiotracer for imaging fatty acid amide hydrolase by positron emission tomography. *Nucl Med Biol*. 2011;38:247–253.
35. Wyffels L, Muccioli GG, Kapanda CN, et al. PET imaging of fatty acid amide hydrolase in the brain: synthesis and biological evaluation of an ¹¹C-labelled URB597 analogue. *Nucl Med Biol*. 2010;37:665–675.
36. Rotstein BH, Wey HY, Shoup TM, et al. PET imaging of fatty acid amide hydrolase with [¹⁸F]DOPP in nonhuman primates. *Mol Pharm*. 2014;11:3832–13828.
37. Sadovski O, Hicks JW, Parkes J, et al. Development and characterization of a promising fluorine-18 labelled radiopharmaceutical for in vivo imaging of fatty acid amide hydrolase. *Bioorg Med Chem*. 2013;21:4351–4357.
38. Hicks JW, Parkes J, Sadovski O, et al. Synthesis and preclinical evaluation of [¹¹C-carbonyl]PF-04457845 for neuroimaging of fatty acid amide hydrolase. *Nucl Med Biol*. 2013;40:740–746.
39. Skaddan MB, Zhang L, Johnson DS, et al. The synthesis and in vivo evaluation of [¹⁸F]PF-9811: a novel PET ligand for imaging brain fatty acid amide hydrolase (FAAH). *Nucl Med Biol*. 2012;39:1058–1067.
40. Pike VW. PET radiotracers: crossing the blood-brain barrier and surviving metabolism. *Trends Pharmacol Sci*. 2009;30:431–440.
41. Innis RB, Cunningham VJ, Delforge J, et al. Consensus nomenclature for in vivo imaging of reversibly binding radioligands. *J Cerebral Blood Flow Metabol*. 2007;27:1533–1539.
42. Boileau I, Mansouri E, Williams B, et al. Fatty acid amide hydrolase binding in brain of cannabis users: imaging with the novel radiotracer [¹¹C]CURB. *Biol Psychiatry*. 2016;80:691–701.
43. Jacobson MR, Watts JJ, Da Silva T, et al. Fatty acid amide hydrolase is lower in young cannabis users. *Addict Biol*. 2020:e12872.
44. Watts JJ, Jacobson MR, Lalang N, et al. Imaging brain fatty acid amide hydrolase in untreated patients with psychosis. *Biol Psychiatry*. 2020.
45. Kolla NJ, Mizrahi R, Karas K, et al. Elevated fatty acid amide hydrolase in the prefrontal cortex of borderline personality disorder: a [¹¹C]CURB positron emission tomography study. *Neuropsychopharmacol*. 2020:1–8.
46. Liu P, Hamill TG, Chioda M, et al. Discovery of MK-3168: a PET tracer for imaging brain fatty acid amide hydrolase. *ACS Med Chem Lett*. 2013;4:509–513.
47. Wang L, Yui J, Wang Q, et al. Synthesis and preliminary PET imaging studies of a FAAH radiotracer ([¹¹C]MPPO) based on alpha-ketoheterocyclic scaffold. *ACS Chem Neurosci*. 2016;7:109–118.
48. Joshi A, Li W, Sanabria S, et al. Translational studies with [¹¹C]MK-3168, a PET tracer for fatty acid amide hydrolase (FAAH). *J Nucl Med*. 2012;53(S1):397.
49. Postnov A, Schmidt M, Penson J, et al. Kinetic modeling of fatty acid amide hydrolase (FAAH) enzyme occupancy after JNJ42165279 inhibition based on ¹¹C-MK3168 PET imaging of human brain. *J Nucl Med*. 2015;56(S3):362.
50. Hardouin C, Kelso MJ, Romero FA, et al. Structure-activity relationships of alpha-ketooxazole inhibitors of fatty acid amide hydrolase. *J Med Chem*. 2007;50:3359–3368.
51. Mileni M, Garfunkle J, DeMartino JK, et al. Binding and inactivation mechanism of a humanized fatty acid amide hydrolase by alpha-ketoheterocycle inhibitors revealed from cocrystal structures. *J Am Chem Soc*. 2009;131:10497–10506.
52. Apodaca R, Breitenbucher JG, Chambers AL, et al. Oxazolyl piperidine modulators of fatty acid amide hydrolase. US patent application. 2007: WO2007/140005A140002.
53. Timmons A, Seierstad M, Apodaca R, et al. Novel ketooxazole based inhibitors of fatty acid amide hydrolase (FAAH). *Bioorg Med Chem Lett*. 2008;18:2109–2113.
54. Lalit K, Shashi B, Kamal J. The diverse pharmacological importance of indole derivatives: a review. *Int J Pharm Pharm Sci*. 2012;2:23–33.
55. Dadashpour S, Emami S. Indole in the target-based design of anticancer agents: a versatile scaffold with diverse mechanisms. *Eur J Med Chem*. 2018;150:9–29.
56. Zhang L, Villalobos A, Beck EM, et al. Design and selection parameters to accelerate the discovery of novel central nervous system positron emission tomography (PET) ligands and their application in the development of a novel phosphodiesterase 2A PET ligand. *J Med Chem*. 2013;56:4568–4579.
57. Deng X, Rong J, Wang L, et al. Chemistry for positron emission tomography: recent advances in ¹¹C-, ¹⁸F-, ¹³N-, and ¹⁵O-labeling reactions. *Angew Chem Int Ed Engl*. 2019;58:2580–2605.
58. Wilson AA, Jin L, Garcia A, et al. An admonition when measuring the lipophilicity of radiotracers using counting techniques. *Appl Radiat Isot*. 2001;54:203–208.